SCATTER COMPENSATION IN DIGITAL RADIOGRAPHY

Vesa Onnia[1], Vesa Varjonen[2], Mari Lehtimäki[2], Mikko Lehtokangas[1] and Jukka Saarinen[1]

[1] Digital and Computer Systems Laboratory,
Tampere University of Technology
P.O.Box 553, Tampere, FINLAND
Tel: +358 3 365 3876; Fax: +358 3 365 3095
e-mail: vesa.onnia@cs.tut.fi

[2] Oy Imix Ab
Erkkilänkatu 11
33100 Tampere, FINLAND

ABSTRACT

When an X-ray image is taken, interactions between tissues of the patient and X-rays cause scattered radiation. The detection of the scattered radiation causes degradation of the image quality. Very common technique for reducing scatter is the antiscatter grid. The grid is effective, but it can not remove all scattering. Another drawback of the grid is that the dose level must be increased, because of the attenuation caused by the grid. Larger the dose level is, larger the health risk became for the patient. Imaging device could be simplified and the dose level decreased if effects of the scattering could be reduced using computational image processing methods. This paper addresses the problem of the scatter compensation from the digital X-ray images. Our algorithm is based on maximum likelihood expectation maximization (MLEM) algorithm derived in [1]. Modified version of this algorithm is presented in this paper. MLEM algorithm increases noise. Because of this SUSAN filter [13] was used after MLEM. Our algorithm reduced scatter to 21% from its original value in the skull image. Also contrast and signal to noise ratio (SNR) were improved.

1 INTRODUCTION

Contrast loss caused by scattering may be as high as 90% in the mediastinum region [1] and for example, a 12:1 grid at 120 kV reduces mediastinal scatter from 93% to 62% [2]. Computational methods bring new possibilities to do scatter compensation more accurately. There are some research efforts dedicated to the scatter reduction, estimation and measurement [1-12]. Promising results have been given when using so called Bayesian Image Estimation (BIE) method [12]. It has been developed for the digital chest radiographs. It is based on MLEM algorithm [1].

Well known theory [2] says that total exposure is sum of the primary and the scattered radiation. The primary radiation forms important information of the inner structures of the object. The scattering radiation degrades primary information and therefore must be removed. When the scattering radiation is removed using computational methods, two main solution types are used. Method can be based on measurement points of the scatter. Using these points scatter field is interpolated to whole image area and subtracted from total exposure [2,6]. Other method is based on the model of the scatter [1,3-10,12]. Using the theory and the measurements, model is created for the scatter and using it the primary radiation can be determined.

MLEM algorithm [1,2-5,7,12] belongs to model oriented class. Authors of MLEM algorithm have used linear invariant scatter model. It can produce quite good results for thorax images, because the scatter field is relatively smooth in the case of the thorax. But there are some problems if we want to use same method for any kind of objects. The scatter field can be so nonuniform that the linear scatter estimation does not give satisfying results. This is the situation when imaging for example skull. In this paper modified version of MLEM algorithm is presented. It is known that MLEM algorithms decrease SNR. Because of this image must be filtered after scatter compensation. Noise filtering was done using so called smallest univalue segment assimilating nucleus (SUSAN) algorithm [13].

Image acquisition system used in this research is fully digital. Information carried by X-rays is converted to visible light using fluorescent screen. Intensities of this light are read using CCD-array. Principle of the system is shown in Figure 1. CCD-array consists of 2000×2000 semiconductor elements. Resolution of the one element is 0.2×0.2mm. Image data is quantized to 16 bit. Data coming straight from the CCD-array was used rather than data, which is converted to gray scale values. It is easier to perform calculations for this data because values given by CCD-array are linearly dependent on X-ray exposures.

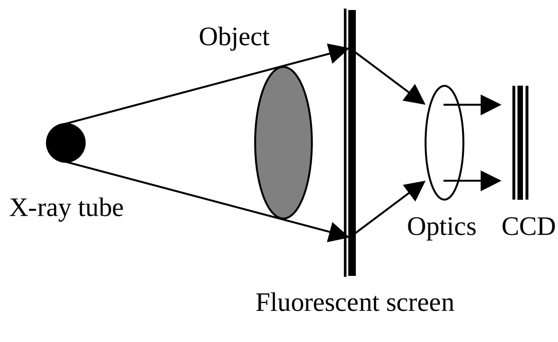

Figure 1. Principle of the digital X-ray imaging system.

2 SCATTER MEASUREMENTS

Scatter was measured using small lead beam stops embedded into polystyrene plate. These beam stops were put into 16×16 matrix, which covered whole image area. Size of one beam stop was 3mm in diameter and 6mm in height. X-rays going straight can not be detected behind the beam-stops. Only the scattered radiation is detected in these points. If film is used when taking X-ray images, so called Posterior Beam Stop (PBS) method can be used [2,9-11]. In PBS method two separate images are taken at the same time: the conventional image and the beam stop image. Using scatter fractions measured from the beam stop image, scatter values in the conventional image can be calculated in the same points. When using fully digital system, two separate images had to be taken: first image, which is a conventional X-ray image taken without the grid and second image, which is taken so that there is the beam-stop matrix between the object and the fluorescent screen. An object to be imaged can not move between these two images because pixels in these images have to be in same places in respect to the object.

Using these two images convolution mask, which produces scatter levels for each pixel depending of its neighbors inside the mask, can be determined. This was done using same method than was used in [10]. Two dimensional radially symmetric exponential scatter kernel was used. Because output of the CCD-array is linearly depended on exposure values, output values could be used without any conversion. Three images were used when the convolution mask was determined: skull, hip and thorax images. We determined only one kernel for all of these images. This kernel produced following root mean square errors (RMSE) between measured and convoluted values: skull 24.43%, hip 51.0776% and thorax 29.47%. If convolution mask is determined individually for each of imaged objects, following results are achieved: skull 24.43%, hip 13.93% and thorax 8.33%. From these results we can see that linear method fits quite well for the scatter estimation in the case of the thorax, but especially skull produces scatter that is difficult to estimate with linear system. In this work we designed the mask, which was determined using all of these images.

3 MLEM ALGORITHM

Areas that cause fast changes to the scatter field, for example boundary area of the skull, are saturated if same MLEM algorithm which has been derived in [1] is used. Linear scatter estimation can not produce satisfactory results. If current estimated scatter is too large with respect to the current estimate of the primary exposure, it must be modified. From the estimated scatter to the estimated primary exposure ratio we get

$$f = \frac{s_k^n}{p_k^n} \Rightarrow s_k^n = p_k^n \cdot f \, , \tag{1}$$

where superscript n denotes nth iteration, subscript k denotes kth pixel, p denotes current estimated primary exposure and s denotes current estimated scatter. Scatter values can be modified by determining some function g which makes coefficient f smaller in the areas where it is too large as follows:

$$s_{kNEW}^n = p_k^n \cdot \frac{f}{g} = \frac{s_k^n}{g} \tag{2}$$

Function g was chosen to be following:

$$g(p_k^n, s_k^n) = \frac{a_1}{\sqrt{2\pi a_2^2}} \exp\left(-a_3 \left(\frac{p_k^n / s_k^n - a_4}{a_2} \right)^2 \right) + 1 \, , \tag{3}$$

where parameters a_1, a_2, a_3 and a_4 are used to set values of g so that better image quality is achieved. These values were searched manually: filtering the image and adjusting the parameters until saturation decreased.

Original MLEM algorithm was

$$p_k^{n+1} = \frac{p_k^n T_k}{p_k^n + \sum_{i=1}^{N} h_{ki} p_i^n} \, , \tag{4}$$

where T denotes measured total exposure, h is convolution mask, h_{ki} denotes mask coefficient that tells how much scattering occurs from pixel i to pixel k and N is total amount of pixels in image. Sum in the denominator is estimated scatter in pixel k on the nth iteration. Now the algorithm becomes following:

$$p_k^{n+1} = \frac{p_k^n T_k}{p_k^n + \dfrac{\sum_{i=1}^{N} h_{ki} p_i^n}{g(p_k^n, \sum_{i=1}^{N} h_{ki} p_i^n)}} \tag{5}$$

Function g is only one alternative and it can be any such function that reduces the level of the estimated scatter in the desired areas. For a's in g following values were found to be good in this case: a_1=1.85, a_2=0.085, a_3=0.015 and a_4=-1.

4 NOISE FILTERING

MLEM algorithm increases SNR [1]. Therefore good noise compensation algorithm is very useful. Noise filtering component is built in to BIE algorithm. In this work MLEM part was separated from BIE and SUSAN noise filtering method was experimented instead of Bayesian approach. SUSAN algorithm is as follows.

$$Y(x,y) = \frac{\sum_{i \neq 0, j \neq 0} I(x+i, y+j) \exp\left(\dfrac{-r^2}{3\sigma^2} - \dfrac{(I(x+i,y+j) - I(x,y))^2}{t^2}\right)}{\exp\left(\dfrac{-r^2}{3\sigma^2} - \dfrac{(I(x+i,y+j) - I(x,y))^2}{t^2}\right)} \tag{6}$$

where Y is filtered image, I is image to be filtered, r is distance between filtered pixel and its neighbor inside determined window, σ controls the scale of the spatial smoothing and t is so called brightness threshold. This equation is applied if the denominator is not zero. Otherwise median is taken from the eight neighbors of the filtered pixel. It must be noticed that sums and median taken over the local neighborhood do not include the filtered pixel itself. If pixel value is near the value of the filtered pixel, it affects much more to the result than if neighbor's value is far from the center value. Because of this property SUSAN algorithm has tendency to preserve significant structures. SUSAN algorithm is performed to the image after the last iteration of the algorithm (5). In this research values σ=0.8 and t=700 were noticed to give good results and window size was 3×3.

5 RESULTS

Signal, noise, SNR and Scatter Removal Accuracy (SRA) were measured. Measurements were done using same methods than in [7]. All three objects, which were imaged, were human type phantoms. Signal, noise and SNR curves (Fig.2-4) were drawn before SUSAN filtering. Curves were drawn for four different places in the image. It can be noticed from figures 1-4 that 10 iterations are enough for MLEM algorithm to converge. There is about 21% left of the scatter in the skull image (Fig.1). This value for the thorax and hip is over 40% for both of them. But if convolution masks which are determined individually for each object type are used, there is about 15% left of the scatter. It can be noticed that these values are not constant for whole image. When SUSAN filtering was done, noise and SNR values were from -7.7% to -28.1% and from 3.6% to 7.8% respectively. Signal values did not changed. Hence SUSAN seems to be quite good noise removal method. Filtered images are shown in figures 5-7.

6 CONCLUSION

The scatter is nonlinear in nature. When imaging thorax scatter estimation can be accurate enough if it is done using some linear estimation method. If estimation must be done for any object of the human body, linear methods for scatter estimation are not accurate enough. Therefore adaptive methods for scatter estimation are needed. We will continue our research in this area.

Another way to do scatter compensation is based on measurements. Scatter is measured from each taken image and using these measurements scatter field is formed and subtracted from total exposure. When using fully digital system, PBS type of methods can not be used. So two separate images must be taken to measure the scattering. This increases the dose level for the patient. However measuring method should not increase health risk for the patient and it should not destroy any information from an image.

REFERENCES

[1] A.H. Baydush, J.E. Bowsher, J.K. Laading, C.E. Floyd, Jr., "Improved Bayesian image estimation for digital chest radiography", Med. Phys., 24, 1997, pp. 539-545.

[2] J.Y. Lo, C.E. Floyd Jr., J.A. Baker, C.E. Ravin, "Scatter Compensation in Digital Chest Radiography Using the Posterior Beam Stop Technique", Med. Phys., 21, 1994, pp. 435-443.

[3] C.E. Floyd, Jr., A.H. Baydush, J.Y. Lo, J.E. Bowsher, C.E. Ravin, "Bayesian restoration of chest radiographs: Scatter compensation with improved signal to noise ratio", Invest. Radiol., vol. 29, 1994, pp. 904-910.

[4] A.H. Baydush, C.E. Floyd, Jr., "Spatially varying Bayesian Image Estimation", Appl. Radiol., 3, 1996, pp. 129-136.

[5] A.H. Baydush, C.E. Floyd, Jr., "Bayesian image estimation of digital chest radiography: Interpedence of noise, resolution and scatter fraction", Med. Phys., 22, 1995, pp. 1255-1261.

[6] K.P. Maher, J.F. Malone, "Computerized scatter correction in diagnostic radiology", Contemp. Phys., vol. 38, 1997, pp. 131-148.

[7] C.E. Floyd, Jr., A.H. Baydush, J.Y. Lo, J.E. Bowsher, C.E. Ravin, "Scatter Compensation for Digital Chest Radiography using Maximum Likelihood Expectation Maximiation", Invest. Radiol., vol. 28, 1993, pp. 427-433.

[8] J.A. Seibert, J.M. Boone, "X-ray scatter removal by deconvolution", Med. Phys., 15, 1988, pp. 567-575.

[9] J.Y. Lo, C.E. Floyd, Jr., J.A. Baker, C.E. Ravin, "An artificial neural network for estimating scatter exposures in portable chest radiography", Med. Phys., 20, 1993, pp. 965-973.

[10] L.A. Love, R.A. Kruger, "Scatter estimation for a digital radiographic system using convolution filtering", Med. Phys., 14, 1987, pp. 178-185.

[11] C.E. Floyd, Jr., J.A. Baker, J.Y. Lo, C.E. Ravin, "Posterior Beam-Stop Method for Scatter Fraction Measurement in Digital Radiography", Invest. Radiol., vol. 27, 1992, pp. 119-123.

[12] A.H. Baydush, J.E. Bowsher, C.E. Ravin, C.E. Floyd, Jr., "Visual improvements in bedside radiographs via numerical compensation", http://deckard.mc.duke.edu/dird/chest/ RSNA97/Bayesian/RAD/ RADframe.html.

[13] S.M. Smith, "SUSAN Low Level Image Processing", http://www.fmrib.ox.ac.uk/~steve/susan/index.html.

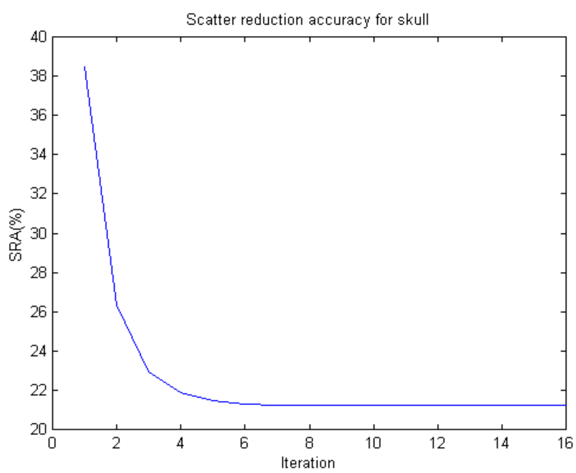

Figure 1. Scatter removal accuracy for skull.

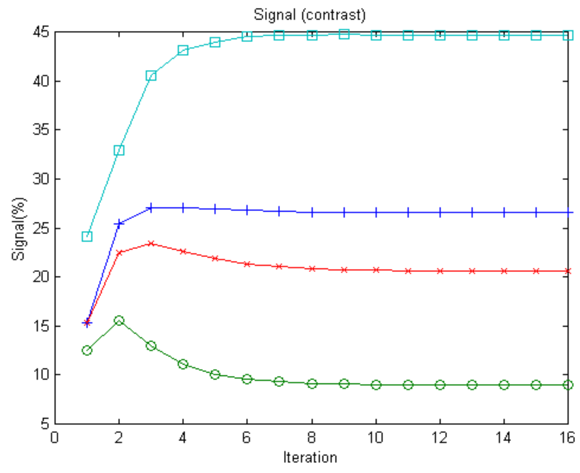

Figure 2. Signal / contrast values for each iteration for skull. *)

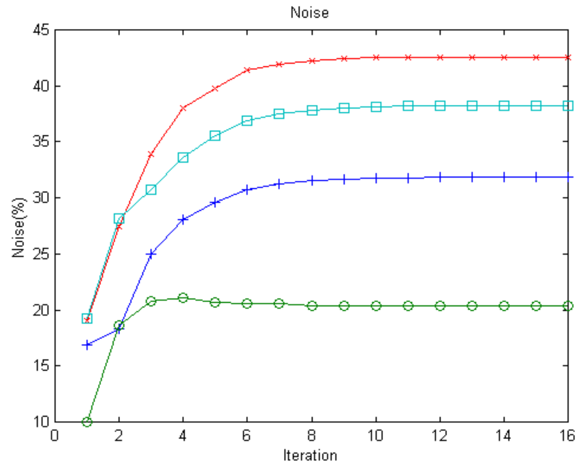

Figure 3. Noise values for each iteration for skull. *)

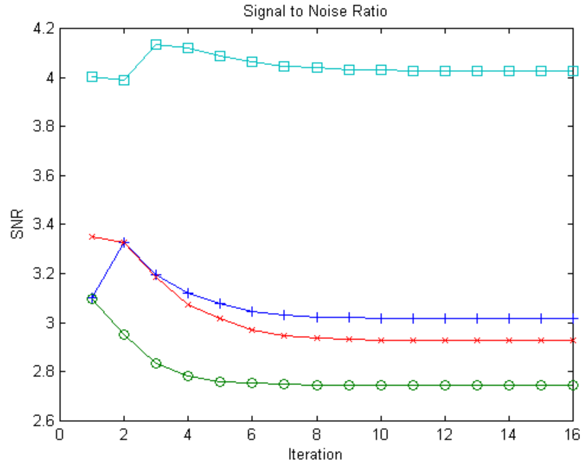

Figure 4. SNR values for each iteration for skull. *)

*) Four different curves were taken from different places in the skull image.

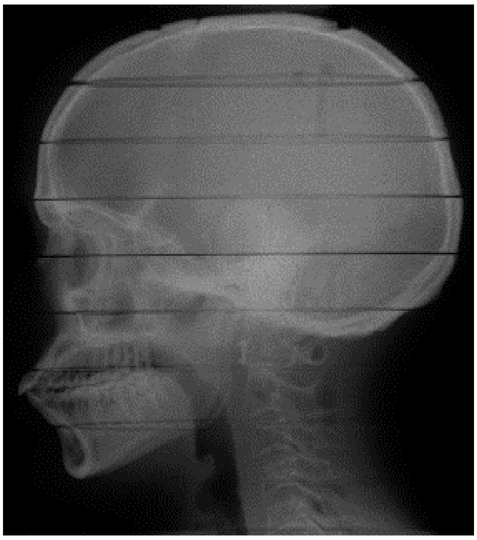

Figure 5. Original skull image.

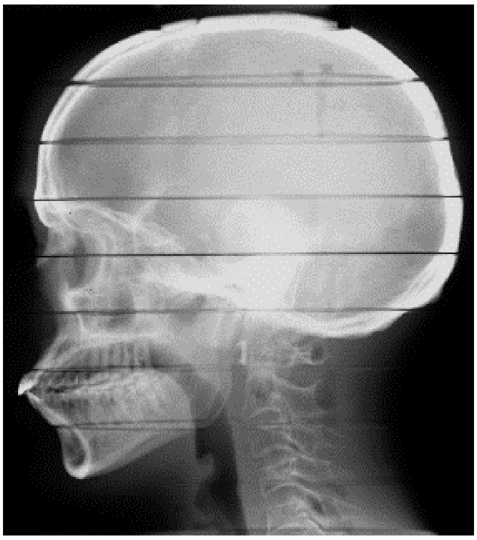

Figure 6. Image filtered using original MLEM

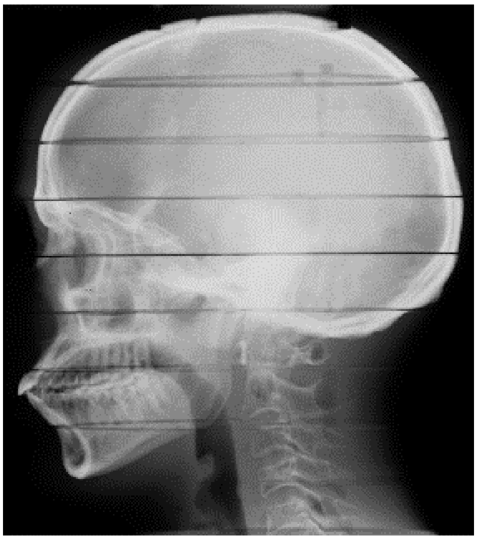

Figure 7. Image filtered using modified MLEM algorithm and SUSAN filter.